Electronic Supplementary Material (ESI) for Soft Matter.

SUPPLEMENTAL INFORMATION

Curvature preference of cubic $CsPbBr_3$ quantum dots embedded onto phospholipid bilayer membranes

Ricki Chairil[a] and Noah Malmstadt[a,b,c]

Affiliations

[a] Mork Family Department of Chemical Engineering and Materials Science, University of Southern California, 925 Bloom Walk, HED 216, Los Angeles, CA 90089, USA

[b] Department of Chemistry, University of Southern California, 3620 McClintock Ave., SGM 418, Los Angeles, CA 90089, USA

[c] Alfred E. Mann Department of Biomedical Engineering, University of Southern California, 925 Bloom Walk, HED 216, Los Angeles, CA 90089, USA

Contents

S1. Detailed overview of Kappa algorithm to obtain curvatures[5]

Briefly, Kappa obtains curvatures *via* the following algorithm:

- The user traces the curved membrane using a series of control points, generating the initialization curve,
- The initialization curve is converted to cubic B-splines, which are piecewise Bézier curves (paramteric curves based on the Bernstein polynomials) connected at their endpoints[3],
- The Böhm algorithm is applied to extract the individual Bézier curves from the B-spline curve, and the de Casteljau algorithm can be applied as needed to bifurcate any Bézier curves for finer curve fitting [2],
- The curvature is calculated *via* the simple relation[7] at a Bézier curve's control points:

$$\kappa(t_0) = \frac{d-1}{d}\frac{h}{a^2} \tag{1}$$

  where $\kappa(t_0)$ = the local curvature at control point t_0, d = the degree of the curve (in this case, 3), a = the length of the line segment connecting the first two control points, and h = the perpendicular distance between the third control point and the secant line passing through the first two control points,

- New endpoints are created from subsequent application of the Böhm and de Casteljau algorithms, so the two above steps are repeated until the entire curve's curvature is characterized.

To minimize selection bias, users can fit a given area around a selection to the specified curve. Kappa performs fitting based on the positions and intensity values in the vicinity of the user's B-spline curve. Point-distance minimization (PDM) or squared distance minimization (SDM) are the two least-squares methods employed by Kappa for surface fitting[4][8]. For all data presented in this work, Kappa's default fitting sensitivity was employed.

This entire curvature acquisition algorithm is given in the preprint article, *Kappa (κ): Analysis of Curvature in Biological Image Data using B-splines*, by Dr. Hadrien Mary and Prof. Gary Brouhard, uploaded in 2019 to bioRχiv[5].

S2. Temperature effect on $CsPbBr_3$-embedded non-deformed GUV curvature-intensity distributions

To ascertain the impact of temperature and potential steric effects on the membrane partitioning of quasispherical $CsPbBr_3$, non-deformed $CsPbBr_3$-embedded GUVs as described in the main text were first imaged at room temperature (21°C) in Skyes-Moore chambers. They were then gradually heated using an Okolab H402-KF-T&C hotplate attachment to the Okolab controller's maximum temperature of 50°C. Thermocouple measurement indicated the actual GUV solution temperature was around 42°C, slightly higher than the gelling temperature of DPPC. This temperature was then maintained for 75 minutes, and then the vesicles were imaged again. Figure S1 gives the resulting images and individual curvature-intensity distributions. There is no statistically significant difference between those distributions even after 75 minutes of thermally fluidizing the membrane.

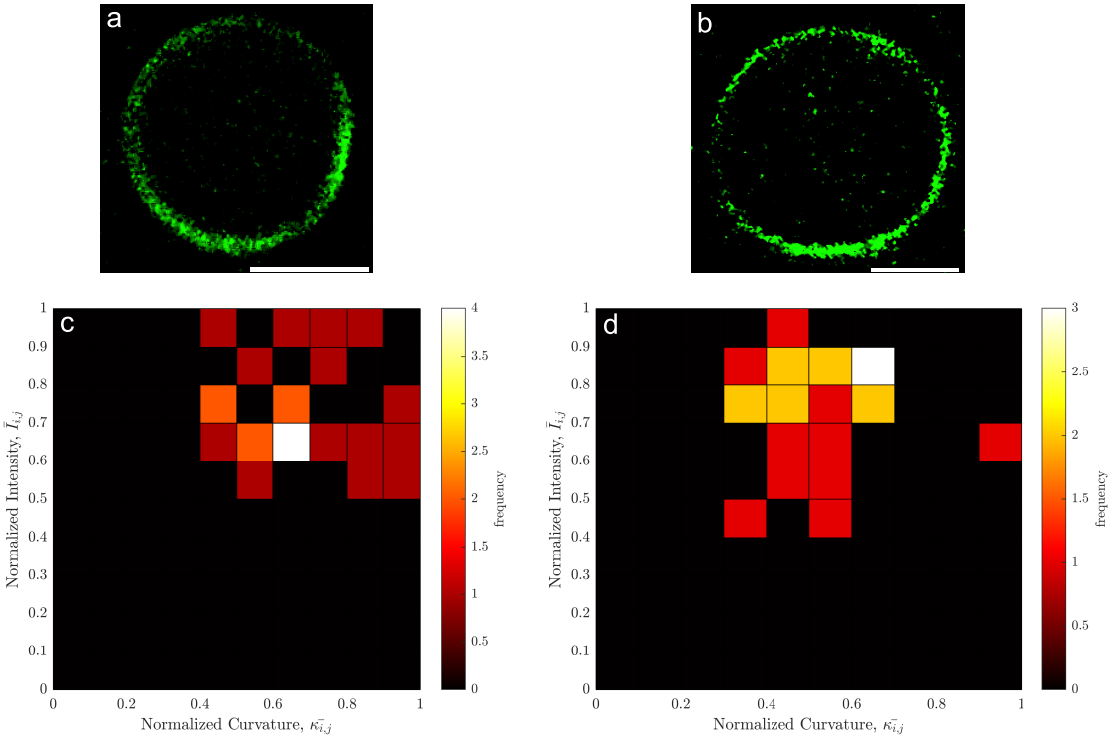

Figure S1: Representative microscopy images of $CsPbBr_3$-embedded DPPC GUVs (a) at 21°C, and (b) after 75 minutes of maintained heating at 42°C. Scale bars are 10 μm. Bivariate histograms of the vesicles are also shown: (c) before heating, and (d) after 75 minutes at 42°C. A 2D Kolmogorov-Smirnov test (before heating sample size $n_1 = 24$, after heating sample size $n_2 = 23$) indicated that there is no statistically significant difference ($p = 0.0785$, $D_n = 0.487$) between the distribution shown in (c) vs that shown in (d).

S3. Temperature effect on $CsPbBr_3$-embedded deformed GUV curvature-intensity distributions

The same temperature-dependent experiments as described in the previous section were performed using deformed $CsPbBr_3$-embedded GUVs as described in the main text. Briefly, these deformed GUVs were first imaged at room temperature (21°C) in Skyes-Moore chambers. They were then gradually heated using an Okolab H402-KF-T&C hotplate attachment to the Okolab controller's maximum temperature of 50°C. Thermocouple measurement indicated the actual GUV solution temperature was around 42°C, slightly higher than the gelling temperature of DPPC. This temperature was then maintained for 45 minutes, and then the vesicles were imaged again. Figure S2 gives resulting representative vesicle images and individual curvature-intensity distributions. Due to convective movement of the vesicles during heating, it was difficult to track individual vesicles, so multiple candidate vesicles (2 before, 3 after) were taken as representatives of the before and after heating conditions. There is a statistically significant difference between those distributions, indicating that the curvature partitioning of $CsPbBr_3$ is likely dependent on the vesicle lipid phase.

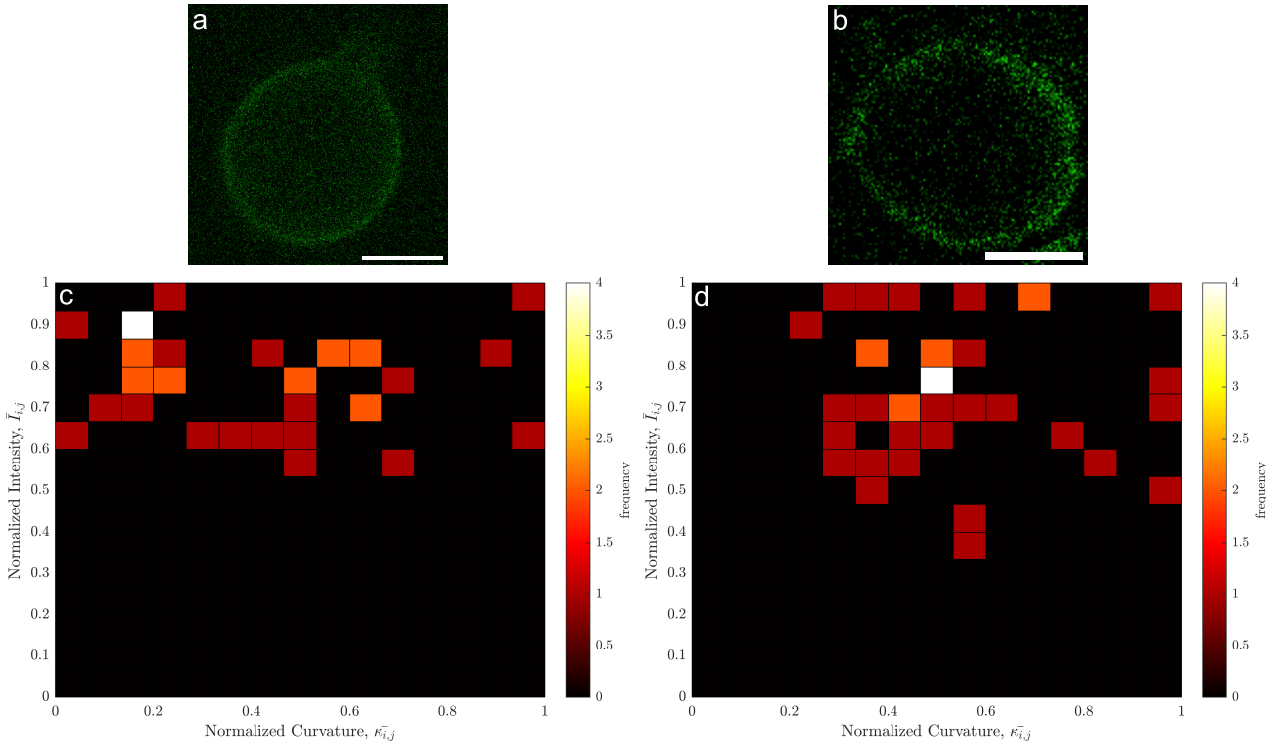

Figure S2: Representative microscopy images of $CsPbBr_3$-embedded DPPC GUVs (a) at 21°C, and (b) after 45 minutes of maintained heating at 42°C. Scale bars are 10 μm. Bivariate histograms of the vesicles are also shown: (c) before heating, and (d) after 75 minutes at 42°C. A 2D Kolmogorov-Smirnov test (before heating sample size $n_1 = 35$, after heating sample size $n_2 = 40$) indicated that there is a statistically significant difference ($p = 0.0487$, $D_n = 0.417$) between the distribution shown in (c) vs that shown in (d).

S4. Temperature effect on deformed GUV curvature-intensity distributions, all fluorescent treatments

Next, all three fluorescent species were considered after deformation and heating to beyond the fluid transition temperature of DPPC. Briefly, deformed GUVs embedded with $CsPbBr_3$, ATTO-488, and CdSe were first produced as described in the main text. They were then gradually heated using an Okolab H402-KF-T&C hotplate attachment to the Okolab controller's maximum temperature of 50°C. Thermocouple measurement indicated the actual GUV solution temperature was around 42°C, slightly higher than the gelling temperature of DPPC. This temperature was then maintained for 45 minutes, and then the vesicles were imaged and analyzed in Kappa and MATLAB as described in the main text. Figure S3 gives the resulting curvature-intensity distributions. Due to convective movement of the vesicles during heating, it was difficult to track individual vesicles, so multiple candidate vesicles (3 for $CsPbBr_3$, 2 for ATTO-488, and 2 for CdSe) were taken as representatives. There is a statistically significant difference between the distributions of $CsPbBr_3$ vs. ATTO-488 and CdSe vs ATTO-488 vesicles (see Table S1), indicating that the curvature partitioning of nanoparticles $CsPbBr_3$ and CdSe might be dependent on the vesicle lipid phase, whereas a small fluorophore like ATTO-488 is less dependent on this thermal migration.

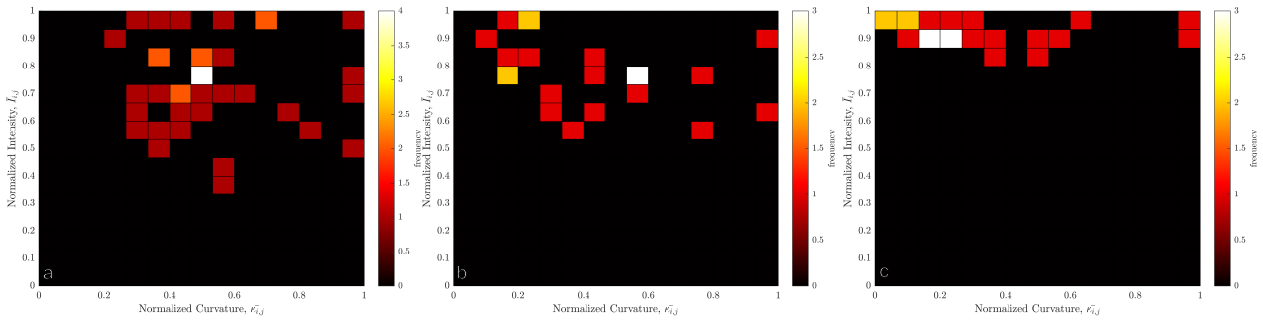

Figure S3: Bivariate histograms of normalized curvature and intensity for deformed GUVs intercalated with (a) $CsPbBr_3$ (sample size $n = 40$), (b) CdSe (sample size $n = 22$), and (c) ATTO-488 (sample size $n = 23$) after 45 minutes of maintained heating at 42°C.

Table S1: Two-dimensional Kolmogorov-Smirnov test statistics D_n and estimated p-value on fluorescent-tagged GUVs after deformation and sustained heating to 42°C.

Comparison	D_n	p-value
$CsPbBr_3$ *vs.* ATTO-488	0.713	$2.89 \cdot 10^{-5}$
$CsPbBr_3$ *vs.* CdSe	0.359	0.365
CdSe *vs.* ATTO-488	0.731	$2.75 \cdot 10^{-4}$

S5. Bivariate histograms for the representative GUVs shown in Fig. 2

The bivariate heatmaps for the nine model GUVs (three of each fluorophore treatment) shown in Fig. 2 in the main text are given in Fig. S4(a) to (i). A detailed mapping of the image of deformed $CsPbBr_3$ vesicle shown in Fig. 2(a) to its corresponding histogram is shown in Fig. S4(j).

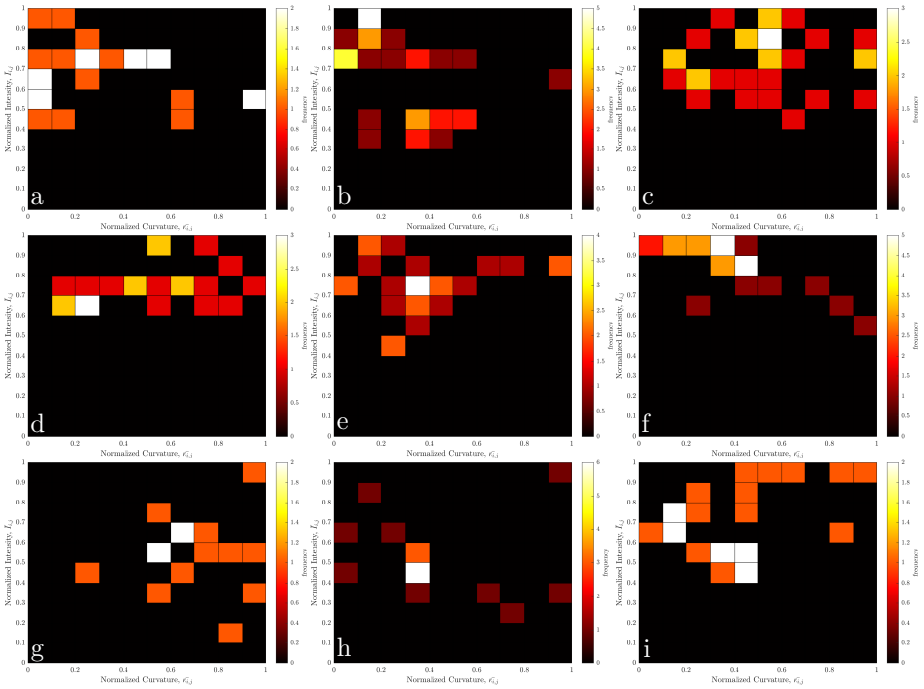

Figure S4: Above, bivariate histograms of normalized curvature and intensity for deformed GUVs embedded with (a)-(c) $CsPbBr_3$, (d)-(f) ATTO-488, and (g)-(i) CdSe. The vesicle from Fig. 2(a) has histogram Fig. S4(a), the vesicle from Fig. 2(b) has histogram Fig. S4(b), and so forth. Below, Fig. S4(j) shows four selected points (I)-(IV) along the membrane of the vesicle from Fig. 2(a), and links them to their corresponding bins on its 2D curvature-intensity histogram. Ordered pairs represent the (normalized curvature, normalized intensity) at the corresponding point as calculated by Kappa. Scale bar is 10 μm.

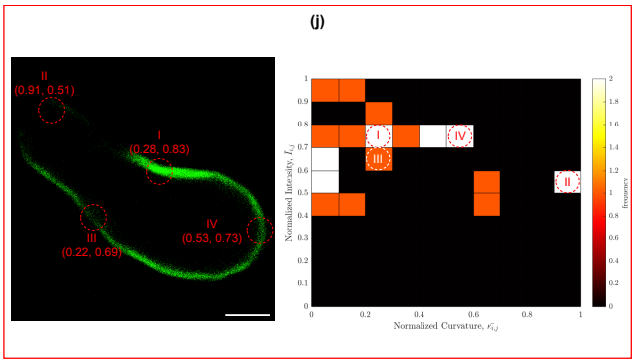

S6. Observed CdSe QD clustering on some GUV membranes

Following Section 3.3 of the article main text, extreme clustering of CdSe was observed for some (30%) GUVs, regardless of whether or not membrane deformation was applied. These can be observed in Figure S5.

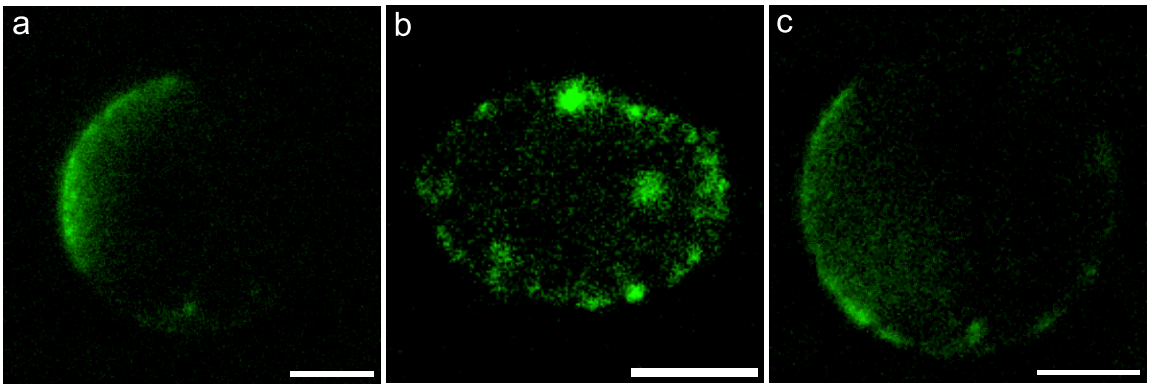

Figure S5: Selected examples of CdSe clustering along DPPC membranes of (a) and (c): non-deformed, (quasi)spherical GUVs, and (b): deformed GUV. Scale bars are 10 μm. Vesicles with these intense (i.e. greater than micron-scale) clustering features were excluded from all curvature-intensity analyses. Scale bars are 10 μm.

S7. Effect of positive- and negative-principal curvature on intensity distributions

The simplified thermodynamic model considered in Section 3.7 of the main text neglects Gaussian curvature. To justify this assumption, we may examine the effect the sign of the absolute curvature may have on the intensity distributions. This can be performed by dividing the three fluorescent treatment ($CsPbBr_3$, CdSe, and ATTO-488) into sub-datasets; these sub-datasets were then normalized via Eqs. 1-2 in the main text. The respective values of $|\kappa_{max,j}|$ and $I_{max,j}$ for all sub-datasets were left unchanged, and thus all references to the maximal curvature and intensity values on the original parent vesicles were retained. Figure S6 gives the resulting normalized curvature-intensity distributions. There is no statistically significant difference ($p > 0.05$) between the negative absolute curvature-only and positive absolute curvature-only fluorescence distributions of $CsPbBr_3$ and ATTO-488 vesicles (see Table S2), indicating that the fluorescence intensity does not depend on the sign of the principal curvatures, and hence the energetic contribution of the Gaussian curvature may be neglected. The p-value for the CdSe positive-only vs. negative-only data was less than 0.05, but this is perhaps due to the lower sample size for the CdSe datasets compared to those for $CsPbBr_3$ or ATTO-488, in light of the behavior of the sign-dependent distributions of the other two treatments, and due to the (acceptably small) sub-micron scale QMC-QLC type aggregation behavior described in Section 3.3 of the main text.

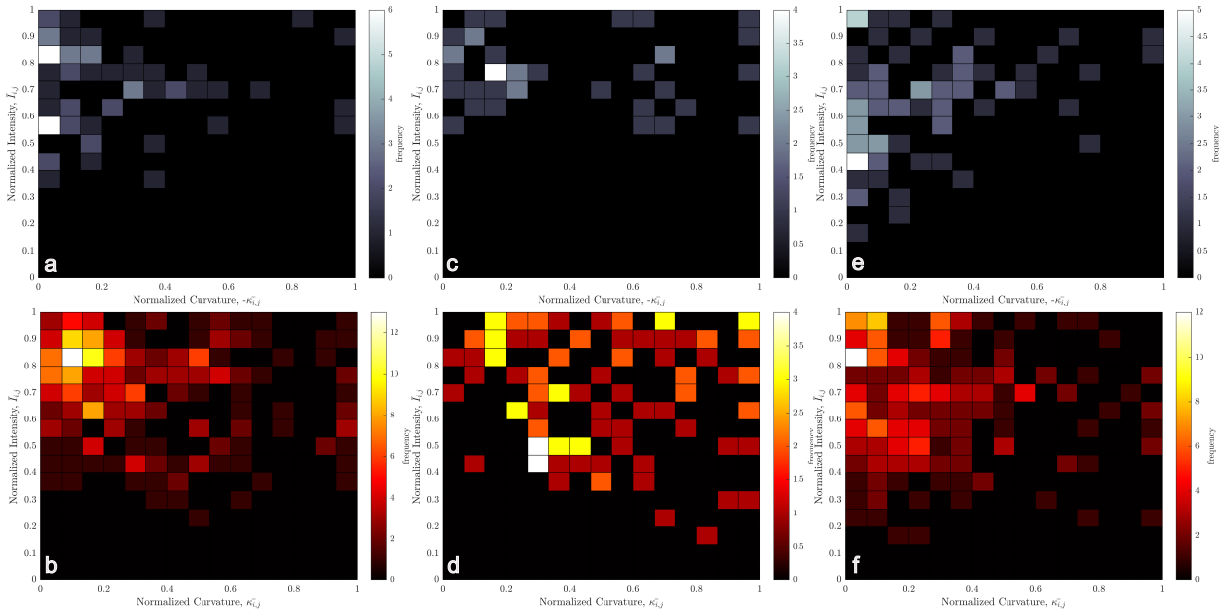

Figure S6: Bivariate histograms of normalized curvature and intensity for deformed GUVs, sorted into negative and positive principal curvature sub-datasets. (a) Negative principal curvatures only, for $CsPbBr_3$-embedded GUVs, (b) Positive principal curvatures only, for $CsPbBr_3$-embedded GUVs (sample size $n = 67$ for negative values, 247 for positive values); (c) Negative principal curvatures only, for CdSe-embedded GUVs, (d) Positive principal curvatures only, for CdSe-embedded GUVs (sample size $n = 41$ for negative values, 101 for positive values); (e) Negative principal curvatures only, for ATTO-488-embedded GUVs, (f) Positive principal curvatures only, for ATTO-488-embedded GUVs (sample size $n = 83$ for negative values, 247 for positive values).

Table S2: Two-dimensional Kolmogorov-Smirnov test statistics D_n and estimated p-value on the signed curvature-intensity distributions shown in Figure S6.

Comparison	D_n	p-value
-$CsPbBr_3$ *vs.* +$CsPbBr_3$ (Fig S6(a) vs (b))	0.239	0.078
-CdSe *vs.* +CdSe (Fig S6(c) vs (d))	0.379	0.013
-ATTO *vs.* +ATTO (Fig S6(e) vs (f))	0.233	0.051

S8. Schematic of bending energy model

Figure S7 gives a visualization of the bending energy model and predicted results assuming equal thermodynamic favorability for the cube (C, $CsPbBr_3$)- and sphere (S, CdSe)-packed cases.

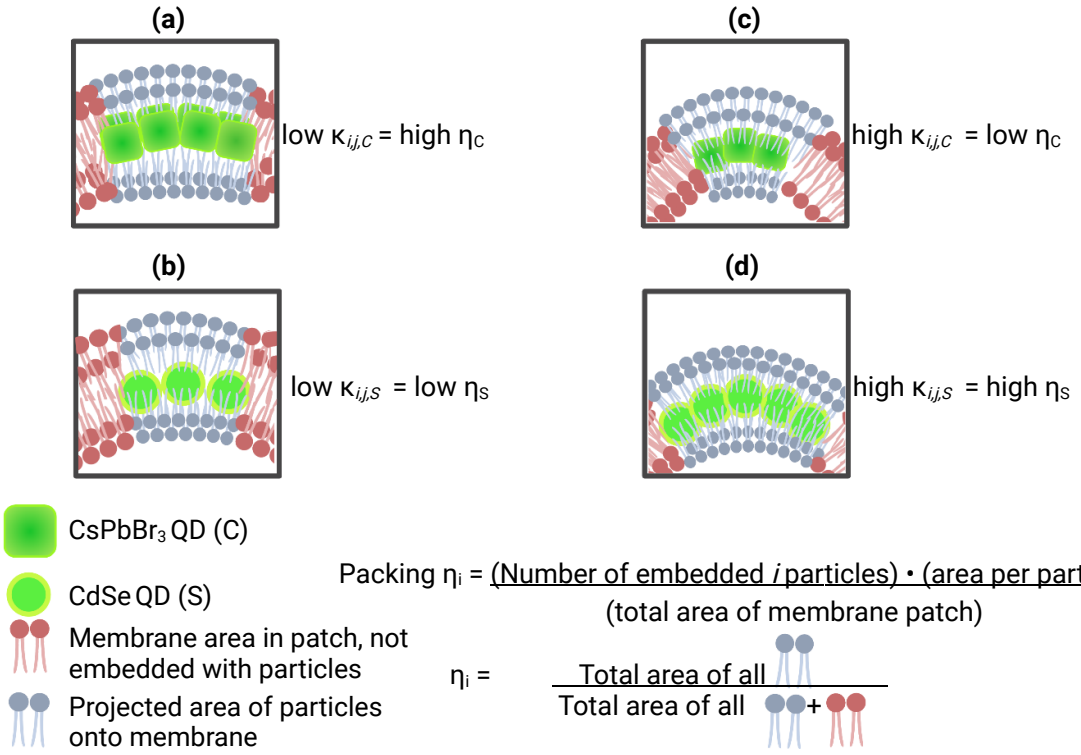

Figure S7: Illustration[1] of the four packed cases of local membrane patches, bounded by the gray boxes, considered in the theoretical model posed by Section 3.7 of the main text - (a) low membrane curvature packed with cubes (e.g. $CsPbBr_3$), (b) low membrane curvature packed with spheres (e.g. CdSe), (c) high membrane curvature packed with cubes, (d) high membrane curvature packed with spheres. The packing predictions are given for each case. As a visual aid, the total area of embedded nanoparticles is represented by the total number of gray phospholipid icons, whereas free phospholipid not in the vicinity of embedded particles but still within the considered patch is given by the red phospholipid icons. These figures are not necessarily drawn to scale and are presented for illustrative purposes only.

S9. Auxiliary MATLAB code for data analysis and visualization

MATLAB code for generation of curvature-intensity heatmaps and profiles based on membrane position can be found on Github: `https://github.com/rchairil/GUV-curvature-study.git`

The quantitative comparison of two curvature-intensity distributions requires use of the `kstest_2s_2d(x1, x2, alpha)` MATLAB function available here[6]: `https://www.mathworks.com/matlabcentral/fileexchange/38617-kstest_2s_2d-x1-x2-alpha`

References

[1] Created with biorender.com.

[2] W. Böhm. Generating the bézier points of b-spline curves and surfaces. *Comput. Aided Des.*, 13(6):365–366, 1981. Special Issue Design optimization.

[3] P. J. Davis. In *Interpolation Approximation*. Dover Publications, Inc., 1975.

[4] J. Hoschek. Intrinsic parametrization for approximation. *Comput. Aided Geom. Des.*, 5(1):27–31, 1988.

[5] H. Mary and G. J. Brouhard. Kappa (κ): Analysis of Curvature in Biological Image Data using B-splines. *bioRxiv*, (852772):1–14, 2019.

[6] D. Muir. kstest_2s_2d(x1,x2,alpha). `https://www.mathworks.com/matlabcentral/fileexchange/38617-kstest_2s_2d-x1-x2-alpha`. Online; accessed 19 Feb 2023.

[7] P. Sederberg. In *Computer aided geometric design*. Dover Publications, Inc., 2012.

[8] W. Wang, H. Pottmann, and Y. Liu. Fitting b-spline curves to point clouds by curvature-based squared distance minimization. *ACM Trans. Graph.*, 25(2):214–238, apr 2006.